Extended line positions, intensities, empirical lower state energies and quantum assignments of NH3 from 6300 to 7000 cm(−1)

ARTICLE *in* JOURNAL OF QUANTITATIVE SPECTROSCOPY AND RADIATIVE TRANSFER · JULY 2012

Impact Factor: 2.65 · DOI: 10.1016/j.jqsrt.2012.02.037

7 AUTHORS, INCLUDING:

Xinchuan Huang
SETI Institute
85 PUBLICATIONS **2,103** CITATIONS
SEE PROFILE

David W. Schwenke
NASA
256 PUBLICATIONS **7,143** CITATIONS
SEE PROFILE

Stephen L. Coy
Massachusetts Institute of Technology
94 PUBLICATIONS **1,745** CITATIONS
SEE PROFILE

Kevin Lehmann
University of Virginia
244 PUBLICATIONS **5,860** CITATIONS
SEE PROFILE

Journal of Quantitative Spectroscopy & Radiative Transfer 113 (2012) 1066–1083

Contents lists available at SciVerse ScienceDirect

Journal of Quantitative Spectroscopy & Radiative Transfer

journal homepage: www.elsevier.com/locate/jqsrt

Extended line positions, intensities, empirical lower state energies and quantum assignments of NH_3 from 6300 to 7000 cm^{-1}

Keeyoon Sung [a,*], Linda R. Brown [a], Xinchuan Huang [b], David W. Schwenke [c], Timothy J. Lee [c], Stephen L. Coy [a], Kevin K. Lehmann [d]

[a] Jet Propulsion Laboratory, California Institute of Technology, Pasadena, CA 91109, USA
[b] SETI Institute, Mountain View, CA 94043, USA
[c] NASA Ames Research Center, Moffett Field, CA 94035, USA
[d] Department of Chemistry, University of Virginia, Charlottesville, VA 22904, USA

ARTICLE INFO

Available online 3 March 2012

Keywords:
Ammonia
Positions
Intensities
Empirical lower and upper state energies
Near infrared

ABSTRACT

Nearly 4800 features of ammonia between 6300 and 7000 cm^{-1} with intensities $\geq 4\times10^{-24}$ $cm^{-1}/(molecule\cdot cm^{-2})$ at 296 K were measured using 16 pure NH_3 spectra recorded at various temperatures (296–185 K) with the McMath–Pierce Fourier Transform Spectrometer at Kitt Peak National Observatory, AZ. The line positions and intensities were retrieved by fitting individual spectra based on a Voigt line shape profile and then averaging the values to form the experimental linelist. The integrated intensity of the region was 4.68×10^{-19} $cm^{-1}/(molecule\cdot cm^{-2})$ at 296 K. Empirical lower state energies were also estimated for 3567 absorption line features using line intensities retrieved from 10 spectra recorded at gas temperature between 185 and 233 K. Finally, using **G**round **S**tate **C**ombination **D**ifferences (GSCDs) and the empirical lower state energy estimates, the quantum assignments were determined for 1096 transitions in the room temperature linelist, along with empirical upper state energies for 434 levels. The assignments correspond to seven vibrational states, as confirmed from recent *ab initio* calculations. The resulting composite database of $^{14}NH_3$ line parameters will provide experimental constraints to *ab initio* calculations and support remote sensing of gaseous bodies including the atmospheres of Earth, (exo)planets, brown dwarfs, and other astrophysical environments.

1. Introduction

Atmospheric ammonia is one of the earliest molecules detected in Jupiter by spectroscopic observations in the visible (6450 Å) by Wildt [1]. Decades later, Gillett et al. [2] detected ν_2 Q branches of NH_3 at 10 μm and confirmed that it is an important opacity source for Jupiter. Subsequent spacecraft observations, such as **IRIS** on Voyager [3], **NIMS** on Galileo [4,5], **CIRS** on Cassini [6], and ground-based data have revealed that NH_3 is ubiquitous in the Jovian atmosphere. It is also detected in low mass brown dwarfs [7–9] and is expected in extrasolar planets [10,11].

Spectroscopic study of atmospheric ammonia (NH_3), one of the simplest hydride molecules and ever present in the primordial gas clouds from which planets are formed, has many facets. In laboratory environments, it leaves unwanted permanent residues on surfaces of absorption cells and optics. Characterizing its infrared spectrum, either with *ab initio* calculations [12–17] or semi-empirical Hamiltonian modeling [18–21] is challenging, particularly at short wavelength because so many ro-vibrational perturbations can occur simultaneously. However, it is an important molecule

* Corresponding author. Tel.: +1 818 354 5144; fax: +1 818 354 0966.
E-mail addresses: keeyoon.sung@jpl.nasa.gov, ksung@jpl.nasa.gov (K. Sung), xinchuan.huang-1@nasa.gov (X. Huang).

0022-4073/$ - see front matter © 2012 Elsevier Ltd. All rights reserved.
doi:10.1016/j.jqsrt.2012.02.037

to astronomers interpreting spectroscopic observations because NH_3 features can be a robust temperature sensor in the atmospheric remote sensing of outer planets, exoplanets, and other astrophysical environments as well as a significant species in study of the chemical and physical processes in the atmospheres.

The longer wavelength side of the 1.5 μm interval is one of the three most important atmospheric windows (*J*, *H*, *K* bands) in the study of extrasolar planets for ground-based observations because it is relatively free of terrestrial absorptions. This region contains prominent NH_3 bands, but unfortunately, the NH_3 spectroscopy is seriously lacking (the line parameters are completely missing in the HITRAN [22] and GEISA database [23]). Thus astronomers have relied on inadequate band parameters and *k*-coefficients based on low resolution cross sections in the 4000–11,000 cm^{-1} (0.9–2.5 μm) obtained from laboratory spectra [24,25] using Goody band models [26]. At 1.5 μm, significant discrepancies were seen from their own measurements by more than 10% when converted to low temperatures [24]. However, since each 'bin' of a cross section may be composed of hundreds of individual transitions having a wide range of lower states, this approach has intrinsic limitations in calculating correct opacities over the wide range of hot and cold temperatures encountered in planetary atmospheres. Better accuracies can be secured by correctly modeling radiative transfer processes through line by line calculations, which requires at a minimum four important spectroscopic line parameters: line position, line intensity, lower state energy, and pressure-broadening coefficient for each line. Theoretical predictions of these parameters can be initiated and validated by laboratory measurements to complete our understanding of NH_3 spectroscopy as a whole.

NH_3 has four fundamental modes (ν_1, ν_2, ν_3, ν_4), all of which are infrared active and show resolved (*a*, *s*) inversion doubling, in addition to the usual vibrational degeneracies ($v_3^{l_3}$, $v_4^{l_4}$ with l_3 and l_4 being vibrationally induced rotational quantum numbers and their effective value $l_{eff}=l_3+l_4$). Its two strongest bands (ν_1 and ν_3) in the 3 μm and another strongly interacting band ($2\nu_4$) dominate the spectrum at 3 μm [21 and the references therein], while their corresponding overtone and combination bands are prominent in the 1.5 μm region. A total of 43 vibrational states have been predicted in the *ab initio* calculations in 6300–7000 cm^{-1} [12,13]. Expected bands in this region are $2\nu_1$, $2\nu_3$ ($|l|=2$, 0), $\nu_1+\nu_3$, $\nu_2+2\nu_4$ ($|l|=2$, 0), $\nu_3+2\nu_4$ ($|l_{eff}|=3$, 1), $\nu_1+2\nu_2+\nu_4$ ($|l|=1$), $2\nu_2+3\nu_4$ ($|l|=3$, 1), $2\nu_1$, $4\nu_4$ ($|l|=4$, 2, 0), $\nu_1+4\nu_2$, $4\nu_2+\nu_3$, $4\nu_2+2\nu_4$ ($|l|=2$, 0), and so on.

In one of the pioneering works at 1.5 μm, Benedict and Plyler [27] expected two parallel bands ($2\nu_1$ and $2\nu_3^0$) and two perpendicular bands ($\nu_1+\nu_3$, $2\nu_3^2$), but observed only perpendicular bands demonstrating that these type bands are dominant this region. One of the breakthroughs came from studies by Coy and Lehmann [28,29] and Lehmann and Coy [30], based on the microwave-infrared double resonance experiments, who reported seven band origins ($\nu_1+2\nu_4^0$, $2\nu_1$, $2\nu_3^0$, $\nu_1+2\nu_4^2$, $\nu_1+\nu_3$, $\nu_3^1+2\nu_4^{-2}$, $2\nu_3^2$) in the 6520–6850 cm^{-1} region quoting the first two bands from an earlier work as well as confirming the perpendicular bands ($\nu_1+\nu_3$, $2\nu_3^2$) reported by Benedict and Plyler [26]. Most of these unpublished assignments from the early collaboration with Coy and Lehmann [28–30] were incorporated in the present work.

Later, Lundsberg-Nielsen et al. [31] presented an extensive set of spectroscopic line parameters using high resolution gas absorption spectra recorded with a FTS (Bruker 120HR) at room temperatures. They measured line positions and molecular absorption coefficients (in units of $cm^{-1}\,Torr^{-1}$) for 1710 lines in the 6400–6900 cm^{-1} region with their stated precision of 0.0005 cm^{-1} and 3×10^6 $cm^{-1}\,Torr^{-1}$, respectively; they assigned 381 lines using the GSCD method and identified them as $\nu_1+\nu_3$ at 6609 cm^{-1} and $2\nu_3^0$ at 6794 cm^{-1}. They did not report the perpendicular band $2\nu_3^2$ at 6849 cm^{-1} suggested by Benedict and Plyler [27].

Later, technical advances in the laser spectrometers, though limited by the bandpass intrinsic to the laser sources, were exploited in the high-resolution rovibrational spectroscopic study of $^{14}NH_3$ at 1.5 μm [32–35]. Berden et al. [32] studied two perpendicular bands and made new assignments or confirmed the earlier assignments [31] for 18 and 9 low J lines from $\nu_1+\nu_3$ and $\nu_1+2\nu_4^2$ bands, respectively. More recently systematic and extensive studies of $^{14}NH_3$ focusing on one or two particular bands at a time in the 6400–6808 cm^{-1} region was conducted by Xu and colleagues [33–35] using both their own spectra from external-cavity tunable diode laser spectrometer with a White type cell and a calibrated FT-IR data set [36], collectively covering four bands ($\nu_1+\nu_3$, $2\nu_3^0$, $\nu_1+2\nu_4^2$, and $\nu_3+2\nu_4^2$). The number of empirical upper state energies proposed for each of the four bands amounts to 135, 47, 56, and 108 levels, respectively, which provided a good initial starting point for extending quantum assignments. Their work also included 21 additional transition assignments for $\nu_1+\nu_3$ [33], 95 transitions for $\nu_1+2\nu_4^2$ [34], and 238 transitions for $\nu_3+2\nu_4^2$ [35] up to $J=10$. In addition, they fitted positions to upper state energies to an isolated-state model with linear Coriolis term, $2C\zeta Kl$, as well as rotational constants, *B* and *C*, and high order centrifugal terms in Eq. (1) by

$$E(J,K)=E_{vib}+BJ(J+1)+(C-B)K^2 - \text{Centrifugal terms} - 2C\sum(\zeta_i l_i)K \quad (1)$$

As expected, however, the uncertainties for predicted upper state energies are in the range of 0.5 cm^{-1} or worse, so we did not attempt any such fits in this work.

Additional measurements of NH_3 line positions and/or intensities are reported without quantum assignments; these include a broad-band FT-IR experiment which obtained a line list of 1117 features [36] and laser spectroscopy focusing on either a few specific lines useful to *in-situ* monitoring of atmospheric NH_3 [37,38] or on very strong lines for metrological reference [39]. However, without knowing accurate lower state energy, their application is somewhat limited for atmospheric monitoring at various temperatures, especially for the region of severe blending in the densely populated transitions (e.g., Q-branches from numerous sub-bands) which are crowded with various

quanta corresponding to a wide range of lower state energies. A summary of earlier measurements and quantum assignments is presented in Table 1 and compared with those from this work. We note that for our combination differences and empirical upper state levels, we use the calculation ground state levels of Urban et al. [40].

Theoretical modeling of near-IR NH_3 bands is intractable for traditional formalisms [41,42], which are obtained as a power series expansion of operators of all normal modes and moments; there are no longer valid due to the large amplitude motion associated with the ν_2 inversion band and anharmonic stretch–bend coupling.

The spectroscopy of $^{14}NH_3$ in this region is still fragmented and incomplete in understanding, lacking the quantum mechanics modeling to fully account for various observed perturbations (e.g. as irregularities in the *a/s* splitting). These arise from (i) Coriolis type interaction between E states and neighboring levels, (ii) resonant interaction with levels of ν_2, (iii) Fermi (and Darling–Dennison) type interaction (e.g., those between $2\nu_4^0$ and ν_1 causing $\nu_3+2\nu_4^0$ and $\nu_1+\nu_3$ to be nearly equal in their band intensities) [27,30,32]. The primary hindrances lay in the lack of inputs from spectroscopic experiments.

The objectives of this work are (1) to present complete measurements of line positions and intensities of $^{14}NH_3$ at room temperature covering more than 99.7% of its opacity in the 6300–7000 cm^{-1} region, (2) use cold temperature data to obtain empirical lower state energies for many of the features, and (3) identify their rotational quantum assignments and tabulate the corresponding empirical upper state energies from the assignments.

Our resulting composite line parameter compilation in electronic form is available as a Supplemental file from the journal. These data will enable better theoretical quantum mechanical modeling (empirical Hamiltonians and empirically improved *ab initio* calculations) for this difficult spectral region of ammonia. The list is also suitable for radiative transfer calculations and high resolution atmospheric remote sensing.

2. Experimental details

We analyzed high resolution spectra of NH_3 and $^{14}NH_3$ recorded at the unapodized resolution of 0.0112–0.0117 from 3000 to 7500 cm^{-1} with the McMath–Pierce FTS located at Kitt Peak National Observatory. Some of these data were used previously to characterize ammonia bands at 2 μm [43] and 3 μm [44]. An overview of the instrumental configuration is given in Table 2. A globar and a quartz-halogen sources, a CaF_2 beam splitter and two matched InSb detectors were utilized to obtain the spectrum of NH_3 over a 4-year period, along with various gas pressures (0.8–20.1 Torr) and temperatures (185–296 K) and five different stainless steel cells, which include a 0.25 m, a 1.5 m, and a coolable 0.8 m single-pass cells, and a 6 m and a coolable 1 m base multipass cells to achieve various absorption path lengths from 0.25 to 24.4 m. The signal/noise ratio of nearly 1000:1 was achieved by coadding individual spectra acquired under the same gas conditions for 70 min or more. The detailed summary of the recorded experimental gas conditions are listed in Table 3, for each spectrum this shows the gas sample pressures, optical path lengths, gas temperatures, minimum and maximum range of line positions and intensities used, the number of retrieved lines used, the gas sample. The calibration factor applied to the wavenumber scale for each spectrum and the name of scans are also listed. The data set provides a good inventory of the NH_3 spectra in various optical densities suitable for measuring line positions and intensities of both strong and weak transitions ($S\sim 4\times 10^{-24}$ $cm^{-1}/(molecule\cdot cm^{-2})$ at 296 K).

Residual H_2O features inside the FTS were used as frequency calibration; these positions had been calibrated against the 2–0 CO [45] in earlier work, and later confirmed using the 3–0 band of CO [46]. In Table 3 are also included the resulting calibration factors applied to the measured line positions from individual spectra. The accuracies of the reference standards [43,45,46] provide absolute calibration of the wavenumber scale of 0.0001 cm^{-1} or better, but for badly blended features, the present line positions can be much worse (0.003 cm^{-1}).

Table 1
A summary of earlier measurements compared to this work.

Region (cm^{-1})	Bands	#obs pos	#intens or abscoef	#empir lower E''	# empir upper E'	# quant asgn	Refs.
6400–6900	$\nu_1+\nu_3$, $2\nu_3^0$	1710	1710			381	[31]
6400–6630	$\nu_1+\nu_3$,$\nu_1+2\nu_4^2$					27	[32]
6460–6522	$\nu_1+\nu_3$, $2\nu_3^0$				(135, 47)[&]	21[$]	[33]
6400–6800	$\nu_1+2\nu_4^2$	95			56	95	[34]
6400–6808	$\nu_3+2\nu_4^2$	239			108	239	[35]
6400–7000		1117	1117				[36]
6526–6538		152	152				[37]
6300–7000	**Seven bands**	**>4800**	**>4800**	**3567**	**434**	**1096**	**This work**

Notes:
(1) #obs. pos, #intens or abscoef, # empir lower E'', #quant asgn, and # empir upper E' represent the number of positions, intensities (or cross sections or absorption coefficients), lower state energies, quantum assignments, and empirical upper state energies, respectively.
(2) [&]The upper state energies were obtained using the earlier assignments [31]. [$]Additional 21 assignments for $\nu_1+\nu_3$ were also reported.
(3) This work also made estimates of empirical lower state energies (see text for details).
(4) # empir upper E' from this work are 137, 55, 78, 118, 34, 8, and 4 for the seven bands, respectively. Dozens of empirical upper state energy levels E' proposed by the earlier work are confirmed or replaced in this work. See text for details.
(5) The seven bands identified in this work are $\nu_1+\nu_3$, $2\nu_3^0$, $\nu_1+2\nu_4^2$, $\nu_3+2\nu_4^2$, $2\nu_3^2$, $\nu_3+2\nu_4^0$, and $2\nu_2+3\nu_4^1$.

Table 2
Experimental configuration for the ammonia study.[a]

Kitt Peak FTS	
IR source	Globar and Quartz halogen lamp
Beam splitter	CaF_2
Resolution	0.011 cm^{-1} (unapodized)
Aperture	8 mm
Detectors	Two LN_2-cooled InSb
Optical band pass	3000–7000; 3800–8000 cm^{-1}
FTS internal pressure	$\leq$ 0.150 Torr (mostly H_2O)
Integration time	70–90 min
Overview of gas and cells	
NH_3 pressure range	0.8–20 Torr (monitored by MKS Baratron gauges)
Gas sample stated purity	99.9% (for both normal NH_3 and $^{14}NH_3$)
Temperature ranges	185–296 K (monitored by thermocouples on cell surface)
Optical path range	0.25–25 m
Gas cells (stainless steel)	Two room temperature Single pass: 0.25, 1.5 m Multipass: 6 m-base Two temperature controlled (cold) Single pass: 0.8 m Multipass: 1 m-base
Cell windows	CaF_2 (wedged)

[a] Specific gas conditions for individual spectra are listed in Table 3.

Table 3
Overview of experimental gas conditions and retrievals for each spectrum.

Pres (Torr)	Path (m)	Temp (K)	Fmin (cm^{-1})	Fmax (cm^{-1})	Smin (cm^{-2} atm^{-1})	Smax (cm^{-2} atm^{-1})	#lines used	ISO	Calibration factor	Scan name
Warm										
2.66	1.50	294.6	6421.2	6987.7	1.0E−03	1.5E−01	1425	E	1.000000418	J87.1.8
1.89	16.40	296.1	6301.1	7026.3	1.0E−04	3.0E−02	5014	E	0.999999976	J99.1.16
1.89	4.34	296.1	6301.1	7022.9	4.0E−04	8.8E−02	2812	E	0.999999976	J99.1.15
10.05	0.25	295.8	6428.2	6987.7	2.0E−03	1.5E−01	871	E	1.000000398	J99.1.14
8.51	0.25	295.8	6443.5	6960.9	1.1E−03	1.5E−01	926	E	1.000000398	J99.1.13
0.80	8.40	296.1	6301.1	7025.0	7.0E−04	1.3E−01	1993	N	1.000000362	J108.3
Cold										
1.97	0.80	189.0	6463.0	6961.0	7.0E−03	2.4E−01	225	E	1.000000366	J90.2.1
1.03	0.80	233.0	6464.4	6950.8	1.3E−02	1.6E−01	442	E	1.000000366	J90.2.2
2.03	0.80	219.0	6463.0	6959.8	7.0E−03	1.7E−01	406	E	1.000000366	J90.2.7
1.47	24.40	211.0	6300.0	7026.1	1.1E−04	2.5E−02	3584	N	1.000000300	J92.1.10
2.03	16.40	200.0	6301.1	7026.1	2.0E−04	2.5E−02	3494	E	1.000000318	J93.1.2
1.07	16.40	192.0	6301.1	7012.0	5.0E−04	5.9E−02	2310	N	1.000000318	J93.1.3
1.77	4.34	220.0	6301.1	6998.2	8.0E−04	8.5E−01	1883	N	1.000000318	J92.1.5
1.77	4.34	185.0	6301.1	6988.4	8.0E−04	9.2E−02	1785	N	1.000000318	J92.1.7
20.00	0.80	220.0	6447.0	6987.7	3.0E−03	1.6E−01	876	N	1.000000367	J90.2.9
1.77	4.34	195.0	6454.9	6960.9	3.0E−03	1.9E−01	774	N	1.000000318	J92.1.6

Notes:

(1) 1 atm=760 Torr=1013 mb; 1 cm^{-2} atm^{-1} at 296 K=4.033 $\times 10^{-20}$ $cm^{-1}/(molecule \cdot cm^{-2})$,
(2) for the intensity ranges (Smin and Smax) E−03 means $\times 10^{-3}$ etc.
(3) for ISO, E=enriched $^{14}NH_3$ and N=normal sample NH_3,
(4) calibration factors for line positions determined using the 2–0 band [45] and H_2O lines at 1.9 μm [43]. The 9th digit after the decimal is not significant.

3. Retrievals of positions, intensities and empirical lower state energies

Line positions and line intensities were retrieved simultaneously from individual spectra using an iterative nonlinear least squares (NLLS) curve fitting techniques [47], which have produced high quality spectroscopic line parameters for various molecules [21–23,43,44]. The curve fitting algorithm adopts a Voigt function for the molecular line shape profile [48] and a *sinc* function with a field-of-view correction for the instrumental line shape function.

3.1. Positions and intensities

For the room temperature spectra, an initial list of line positions and estimated absorption depths required for

our curve fitting software [47] were collected using peak finding algorithms that take first and second derivatives of the apodized and interpolated spectrum. In the spectrum fitting, the individual positions and intensities were adjusted until the differences between the observed and synthetic spectra were converged to a minimum, typically their fitting residuals less than 0.5%. The spectra were fit one at a time in small spectral intervals. An example is shown in Fig. 1.

New features not discerned by the peak finder were added using interactive commands of the software. In the final step, the measured 'raw' positions from each scan were normalized to standard values using the calibration factors listed in Table 3. The retrieved intensities from individual spectra were inspected to search for any large (10%) systematic offsets from the average, and intensities from those scans were scaled accordingly.

To obtain averaged positions and intensities at room temperature, all the individual calibrated retrievals were sorted by the value of position and processed by a custom-made averaging program [47] which groups the measurements of the same features together if they are closer than half of the spectral resolution. The average was computed, the average and individual values were used to compute the root mean square (rms) agreement, and the information was written to form the experimental line list. Values of blended features usually required some manual corrections. If quantum assignments (thus the correct lower state energy) were known, the individual line intensities from each spectrum were first normalized to corresponding values at 296 K before averaging. At this point, assignments were available for only several hundred lines, but as seen in Table 3, the spectra selected for measurement in this region were recorded with gas temperatures near 296 K.

One example of the process is shown in Table 4. The top panel lists individual room temperature retrievals and the resulting averaged line position and intensity, along with the computed experimental rms for the position and %rms for the line intensity (used to estimate measurement precision). Not all available room and cold spectra listed in Table 2 were used for every line; the measurements were filtered by the intensity values to eliminate retrievals for which the absorption depths were observed to be too weak or too strong; the accepted ranges are given by S_{min} and S_{max} in Table 3. The bottom panel shows the empirical lower state energy obtained for the same line position. Using Eq. (2) (described below) and the averaged room temperature intensity in the top panel, we solved for individual lower states E'' using each cold intensity in turn and then computed the average. When individual retrievals deviated too much from an initial average, they are rejected from the averages.

In Fig. 2 is shown an observed spectrum (upper) and the distribution of the measured line intensities (lower) as a function of line position. The vertical axis in the lower plot is log(intensity) with a lower limit of 4×10^{-24} cm^{-1}/(molecule cm^{-2}). The sum of line intensities in the 6300–7000 cm^{-1} is 4.68×10^{-19} cm^{-1}/(molecule cm^{-2}) at 296 K. While our experimental spectra were recorded with both normal and enriched samples of ammonia, we note that none of the strong $^{15}NH_3$ lines reported recently [49,50] is observed in our linelist.

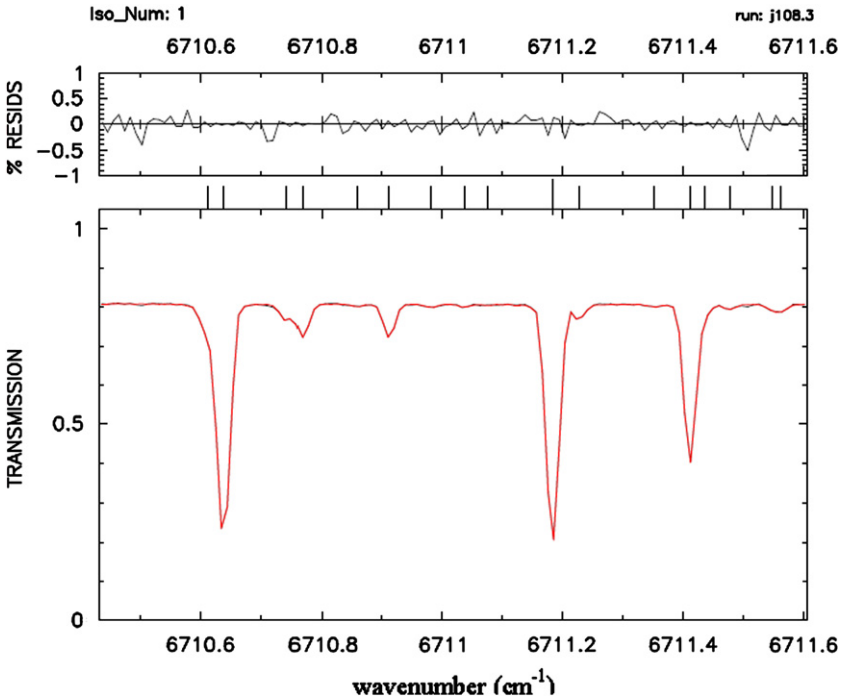

Fig. 1. The upper panel shows excellent agreement between calculated and observed spectra, which are overlaid in the lower panel (**black**=**obs**; **red**=**calc**). The vertical lines between the two panels mark the retrieved features. The spectrum was recorded with P=0.8 Torr, L=8.4 m at 296.1 K at the resolution of 0.0112 cm^{-1} (unapodized). The three largest negative residuals indicate the prescence of weak unmeasured absorptions. (For interpretation of the references to color in this figure legend, the reader is referred to the web version of this article.)

Table 4
Example of averaged position, intensity, and empirical lower state energy.

(A) Averaged position and intensity

Position (cm^{-1})	(av—*n*th) (cm^{-1})	Intensity[a] ($10^{-3} cm^{-2}$ atm^{-1})	%unc	Temp (K)	Path (m)	Pres[a] (Torr)
6576.702782	−0.00008	4.96	3.2	296.1	4.34	1.893
6576.702828	−0.00003	4.66	−3.2	296.1	16.40	1.893
6576.702856	0.00000	4.66	−3.0	296.1	8.40	0.800
6576.702963	0.00011	4.95	3.0	294.4	1.50	2.660

Average position = 6576.70286(7)
Average intensity = 4.81(3.1%) at 296 K

(B) Averaged lower state energy

Position (cm^{-1})	Intensity[a] (10^{-3} cm^{-2} atm^{-1})	Energy (cm^{-1})	%unc	Temp (K)	Path (m)	Pres[a] (Torr)
6576.703121	4.05	489.7	8.0	220.0	0.80	20.000
6576.703707	3.68	468.9	3.4	195.0	4.34	1.770
6576.703791	3.90	426.8	−5.8	185.0	4.34	1.770
6576.703825	4.59	421.8	−6.9	220.0	4.34	1.770
6576.704013	3.99	450.3	−0.6	200.0	16.40	2.030
6576.704160	3.86	444.9	−1.8	192.0	16.40	1.068
6576.704445	4.03	469.9	3.6	211.0	24.40	1.470

Averaged E'' = 498. (5.0%)
Assigned E'' = 521.6220 (7 4 1 0 *s* RQ(7,3)*s* of 1010)[b]

[a] 1 atm = 760 Torr = 1013 mb; 1 cm^{-2} atm^{-1} at 296 K = 4.033×10^{-20} $cm^{-1}/(molecule \cdot cm^{-2})$.
[b] $(J',K',l_3,l_4)s$ $\Delta K \Delta J(J',K')s$ of $\nu_1+\nu_3$.

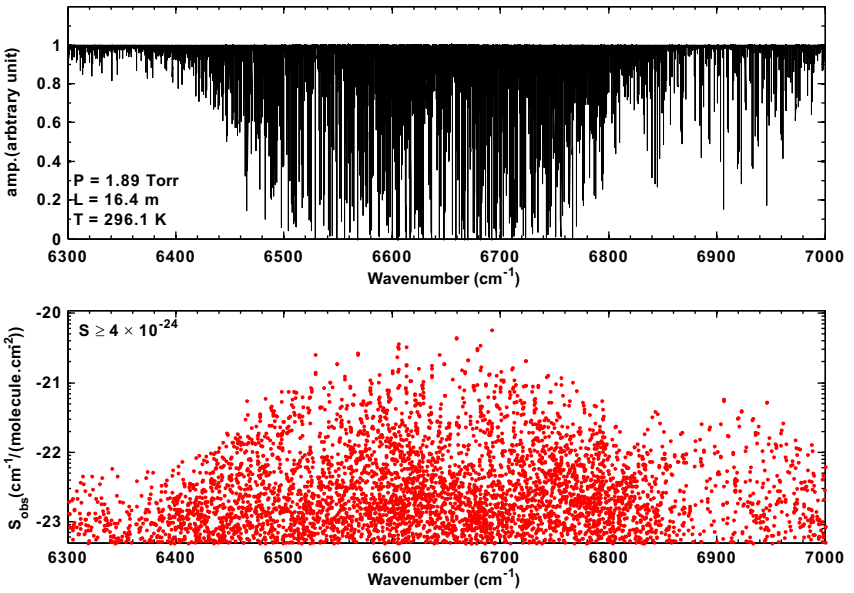

Fig. 2. (*Upper panel*) A sample of Kitt Peak spectra and (*Lower panel*) distribution of measured line intensities against line positions for ~4800 features whose intensities are greater than 4×10^{-24} $cm^{-1}/(molecule \cdot cm^{-2})$ at 296 K. Note that 70 lines are stronger than 1×10^{-21} $cm^{-1}/(molecule \cdot cm^{-2})$. The integrated intensity of 4.68×10^{-19} $cm^{-1}/(molecule \cdot cm^{-2})$ at 296 K represents 99.7% of the observed opacity of $^{14}NH_3$ in this region.

3.2. Estimated empirical lower state energies from cold and room temperature intensities

Once the room temperature linelist is finished, the intensities retrieved from the cold spectra are then used to obtain the experimental estimate of the lower state energy for each observed line using Eq. (2):

$$\frac{S_\nu(T)}{S_\nu(T_o)} = \frac{Q(T_o)}{Q(T)} \exp\left[-E''\left(\frac{1}{kT} - \frac{1}{kT_o}\right)\right] \quad (2)$$

where the ratio of line intensities at two different temperatures T_o and T, lower state energy E'', the partition function Q

(calculated from Gamache et al. [51]), and the Boltzmann constant *k*. However, there were unexpected systematic errors for the gas temperature when the 1-m base multipass cell was cooled; this had been noticed in the prior study of ammonia at 2.0 μm [43] by comparing estimated lower states with calculated values [40] for securely assigned lines of $\nu_3+\nu_4$ near 5050 cm^{-1}. The reason for this was never discovered, but most likely there were problems with the thermocouples embedded in the body of the cell. Using Eq. (2) to well-isolated transitions whose assignments are already well known, we obtained new *effective* temperatures listed in Table 3.

Ground state energies were estimated for 3657 line absorption features, which are presented in Fig. 3. Since this work is limited to a study of bands from only the ground state, their stratified distribution clearly shows the distinctive nature of the ground state energies for NH_3. It should be noted that their color scheme roughly corresponds to the best candidates of *J* values, which are based on the ground state energies derived by Urban et al. [40], as illustrated in Fig. 3. Low values for the empirical lower state energies (e.g., $E<\sim 30\ cm^{-1}$) reveal the lowest *J* transitions (i.e. $J=0$) and in turn approximate centers of bands (and sub-levels); these data provided a complementary constraint to locate new bands and their quantum assignments to be confirmed by *ab initio* calculations.

4. Analysis of quantum assignments

4.1. Transition selection rules

NH_3 bands possess an inversion splitting due to symmetry with respect to the plane of the hydrogens (*s* for symmetric, *a* for asymmetric) producing inversion doublets. The perpendicular bands are vibrationally degenerate requiring additional quantum number *l*. In this region, we use separate *l* values for υ_3 and υ_4. Thus, to unambiguously indicate the upper state levels, we employ nine quantum numbers (υ_1, υ_2, υ_3, υ_4, l_3, l_4, *a/s*, *J*, *K*), and express quantum assignments as $\upsilon_1\ \upsilon_2\ \upsilon_3\ \upsilon_4\ l_3\ l_4$ $\Delta K\Delta J(J,K)a/s$. For **A** type upper states and the ground state, l_3 and l_4 are zero. For the two types of bands, labeled as parallel band (*A*) and perpendicular band (*E*) for cold bands, different selection rules are applied for allowed transitions as summarized in Table 5. For instance, in case of $K=0$, there is no Q-branch (*i.e.*, $\Delta J=0$) for parallel bands, while there is no PQ for perpendicular bands. There are additional selection rules for each, which are nuclear spin weights [52] and perturbation-allowed selection rule. For instance, since the *A* symmetry ro-vibrational states have zero spin weight in NH_3, QP(*J*, 0) is allowed only for odd *J* of symmetric species and even *J* of asymmetric for parallels. In case of perpendicular bands, the standard and perturbation-allowed selection rule, $\Delta(l-K)=0$ and $\Delta(l-K)=3$, respectively, are very strict, so that the rule makes Δl and ΔK additionally inter-coupled in a way that a sub-P branch line ($\Delta K=-1$) should have either $\Delta l=-1$ or $+2$ for allowed transitions. It should be recalled that, for cold bands considered in this work, the lower state, i.e., ground state, does not possess vibrationally induced angular momentum ($l=0$), so that Δl is equal to the upper state *l*.

Typically perpendicular bands are stronger than parallel bands in this region. The stronger branches are expected for $\Delta J=\Delta K$, i.e., PP and RR transitions. From the nuclear spin weights, line intensities with the lower state $K=3$, 6, 9 are enhanced. Such line intensity variations have been used in the quantum assignment as a secondary check in confirming combination differences, as described in the following section.

4.2. Ground state combination differences (GSCDs) to obtain quantum assignments

Using ground state combination differences is a powerful tool to obtain quantum assignments without detailed knowledge from a theoretical calculation. This is

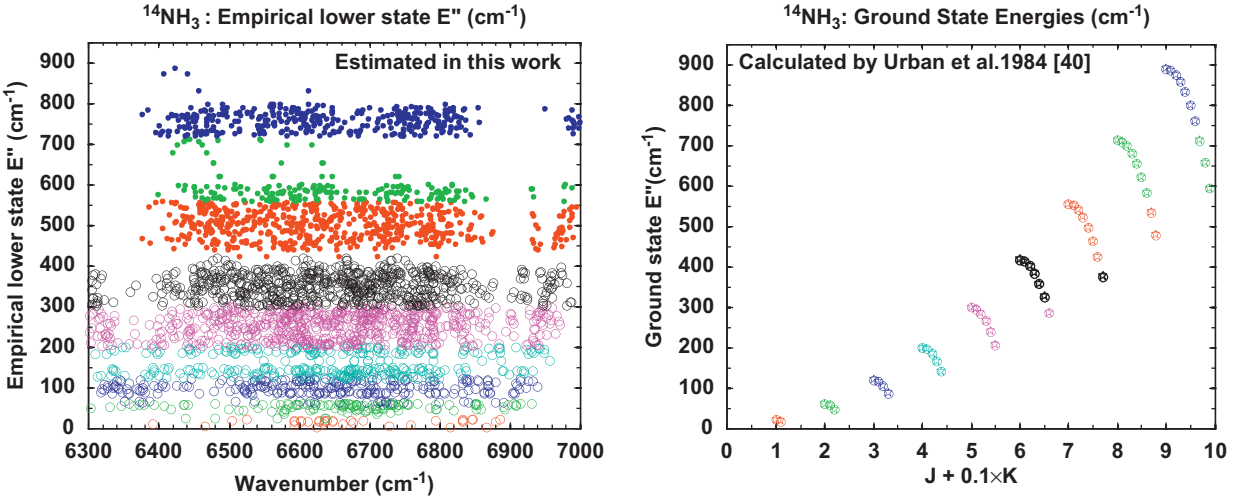

Fig. 3. Comparison of empirical and theoretical ground state energies. (**Left**) Empirical lower state energy estimates from the ratios of intensities measured at various temperatures. Overall uncertainty is estimated to be 5–20%. (**Right**) Distribution of the lower state energies against *J* and *K* adopted from Urban et al. [40]. Good general agreement between empirical and calculated lower states validates the results from the cold data.

Table 5
Transition selection rules of allowed NH_3 transitions used for GSCDs.

Type	Parallel (non-degenerate)	Perpendicular (degenerate)
Species	A	E
Δl	0, ± 3, ± 6,…	± 1, ± 2, ± 4,…
ΔJ and ΔK	For $K=0$, $\Delta K=0$; $\Delta J=\pm 1$	
	For $K\neq 0$, $\Delta K=0$; $\Delta J=0$, ± 1	For all K, $\Delta K=\pm 1$; $\Delta J=0$, ± 1
inversion	$a\leftrightarrow s$	$a\leftrightarrow a$; $s\leftrightarrow s$
$\Delta(l-K)$	0	0, ± 3 (perturbation-allowed)
Nuclear spin weights S for $(J, K)a/s$	$S=2$ for $K=3, 6, 9,\ldots$	
	$S=1$ for $K\neq 3, 6, 9,\ldots$	
	For $K=0$; $S=0$ for even J with s; odd J with a	
	For $K=0$; $S=2$ for odd J with s; even J with a	

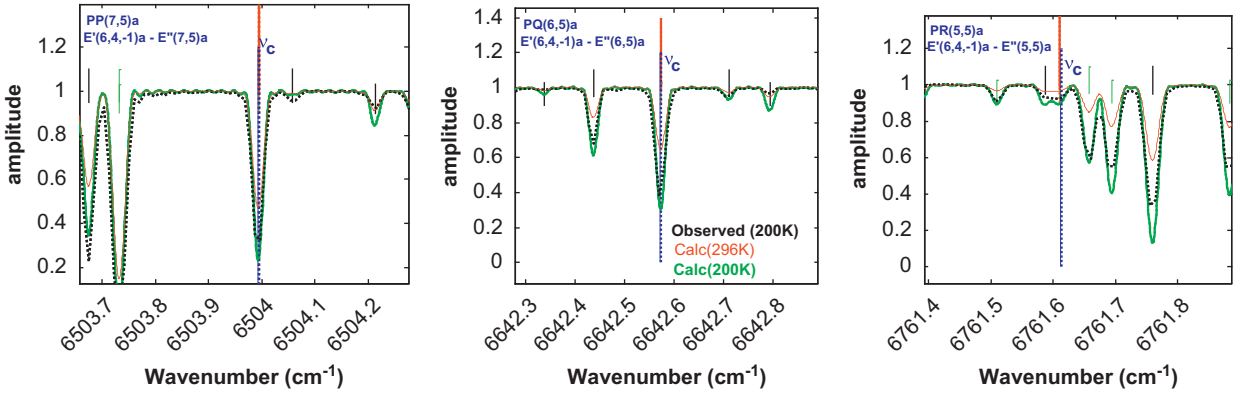

Fig. 4. Confirming quantum assignments using Ground State Combination Differences (GSCDs) and a comparison of calculated lines at 296 K (**red trace**) and 200 K (**green trace**) compared to observed feature at 200 K (**black trace**). The vertical **blue** lines are predicted line centers for this GSCD set. The **green** lines were calculated by scaling intensities at 296 K to 200 K using Eq. (2) and the proposed lower state energies. A good agreement between synthetic and observed spectral line at the cold temperature validated the correct determination of the lower state for the given transitions. The transition PR(5,5)a was ultimately omitted in the upper state energy calculation because the line is blended. (For interpretation of the references to color in this figure legend, the reader is referred to the web version of this article.)

particularly true for NH_3 bands at 1.5 μm because of the structural complexity arising from up to 43 different vibrational sub-bands and a multitude of possible ro-vibrational perturbations between upper state energy levels. The perturbations can ultimately be revealed using validated quantum assignments to improve theoretical calculations [13,14,17].

Using GSCDs, assignments are often considered *confirmed* if several unblended transitions sharing the same upper state level can be identified within the measurement precision of the positions. For instance, with an upper state $E'(J', K')$ of an E type, $\Delta l=-1$ or $+2$ vibrational state, one expects prominent transitions for PP($J'+1$, $K'+1$), PQ(J', $K'+1$), PR($J'-1$, $K'+1$) with the PP($J'+1$, $K'+1$) being the strongest among them. However, where the spectrum is crowded, there is high chance of false matches, and extra care and evaluation should be exercised. In order to determine upper state energies with confidence, we developed a graphical utility to assign lines via GSCD and validate consistencies by simultaneously inspecting (a) the ratio of our estimated lower state energies to the calculated values [40], (b) the ratio of observed and calculated line intensities, in addition to having good agreement between observed and predicted line positions based on updated empirical upper state energies. This provided a mechanism for 'quality control' in the assignment process. The software could be operated interactively, but it also could perform automated searches with a preset tolerance. Examples of this procedure are shown in Fig. 4 and Tables 6 and 7.

Once a GSCD set was accepted, the corresponding empirical upper state energy was computed from the average of observed positions plus calculated ground state values. The 'unblended' lines were used whenever possible. For example in Fig. 4 and Table 6, the rms of the upper state energy based on all the three transitions was 0.00161 cm^{-1}, but it improved to the value of 0.00024 cm^{-1} when the blended PR line is excluded in computing the averaged empirical upper state level E'. Table 7 shows a few samples of the GSCDs, including the one presented in Fig. 4 for Band #1 ($\nu_1+\nu_3$). The entries flagged with asterisk (*) are excluded in computing new upper state energies, but they are retained in the master list of assignments as long as their line intensities look consistent with predictions. The entire list for the GSCDs for seven bands and the details of individual assignments are presented in Appendices A1 and A2, respectively.

Table 6
Examples of GSCD process for Band#1, $\nu_1+\nu_3$ (full list can be found in Appendix A1).

ipOXOX	(J' K' l_3 l_4)s	QN(J'',K'')s	Band.LL	E'(new)	$\langle E'(\text{new})\rangle$	E'rms	E (GS)	wn_obs	wn_cal	wn (o-c)	Sobs296K	E''L/U	Flg	Note
#7 1 1	(6, 4, 1, 0)a	RP(7, 3)a	1010.10	6961.16253	6961.16274	0.00035	522.22303	6438.93950	6438.93977	−0.00027	8.240E−23	0.597	excl	o–k–
#8 1 1	(6, 4, 1, 0)a	RQ(6, 3)a	1010.10	6961.16323	6961.16274	0.00035	383.97756	6577.18567	6577.18524	0.00043	5.082E−22	0.917	excl	o–k–
#9 1 1	(6, 4, 1, 0)a	RR(5, 3)a	1010.10	6961.16246	6961.16274	0.00035	265.22672	6695.93574	6695.93607	−0.00034	1.278E−21	0.973	excl	o–k–
#4 1 1	(6, 4, −1, 0)a	PP(7, 5)a	1010.10	6967.70076	6967.70099	0.00023	463.70721	6503.99355	6503.99379	−0.00024	3.150E−22	0.975	excl	o–k–
#5 1 1	(6, 4, −1, 0)a	PQ(6, 5)a	1010.10	6967.70123	6967.70099	0.00023	325.12739	6642.57383	6642.57361	0.00023	1.900E−22	0.960	excl	o–k–
#6 1 1	(6, 4, −1, 0)a	PR(5, 5)a	1010.10	6967.69755	6967.70099	0.00000	206.08767	6761.60989	6761.61333	−0.00345	1.440E−23	1.470	XCLD	blnd
#7 1 1	(7, 4, 1, 0)s	RP(8, 3)s	1010.10	7098.32511	7098.32477	0.00035	679.28787	6419.03724	6419.03693	0.00031	3.545E−23	0.851	excl	o–k–
#8 1 1	(7, 4, 1, 0)s	RQ(7, 3)s	1010.10	7098.32489	7098.32477	0.00035	521.62204	6576.70286	6576.70276	0.00009	1.940E−22	0.955	excl	o–k–
#9 1 1	(7, 4, 1, 0)s	RR(6, 3)s	1010.10	7098.32429	7098.32477	0.00035	383.31852	6715.00577	6715.00628	−0.00051	5.324E−22	0.968	good	o–k–
#7 1 1	(7, 4, 1, 0)a	RP(8, 3)a	1010.10	7098.07619	7098.07660	0.00029	679.83675	6418.23944	6418.23985	−0.00041	8.389E−23	1.072	excl	o–k–
#8 1 1	(7, 4, 1, 0)a	RQ(7, 3)a	1010.10	7098.07680	7098.07660	0.00029	522.22303	6575.85377	6575.85357	0.00020	3.412E−22	0.946	excl	o–k–
#9 1 1	(7, 4, 1, 0)a	RR(6, 3)a	1010.10	7098.07680	7098.07660	0.00029	383.97756	6714.09924	6714.09904	0.00020	9.437E−22	0.945	excl	o–k–

Notes:

(1) The table columns are as follows:
ipOXOX: quality control parameters used as line index and indicators of allowed and accepted transitions for the GSCD set shown.
(J' $K'$$l_3$ l_4)s QN(J',K')s: upper and lower states.
Band.LL: proposed vibrational band and sub-level, expressed by $n_1n_2n_3n_4.l_3l_4$.
***E′*(new), $\langle E'(\text{new})\rangle$, *E′*rms:** upper state energies computed for an individual line and its averaged value and rms.
E(GS): the ground state energy adopted from Urban et al. [40]
wn_obs, wn_cal, wn(o-c): measured and calculated (*i.e.*, $\langle E'(\text{new})\rangle$ − Edn) line positions and their differences (=wn_obs − wn_cal).
Sobs296K: measured line intensity at 296 K and its ratio to calculated value.
E''**L/U:** ratio of the estimated lower state energy in this work to the ground state energy E(GS), which is a good indicator of the correct assignment.
Flg: flag of line quality: **excl**=excellent while **XCLD**=excluded from the averaged upper state energy.
Note: additional information on the status of the transition.

(2) E'rms=0 means that (1) the upper state energy is determined from one single assignment **or** (2) the lines are excluded in the statistics.
For the latter case, users are advised to use calculated line positions rather than the observed values for a better precision.

(3) The GSCD set presented in Fig. 4 is listed in the second block, which shows the transition PR(5,5)a is omitted in computing the upper state energy.
Nevertheless, it is listed to indicate that an observed line is found in the spectrum.

(4) These proposed band name should be assumed tentative.

Table 7
Examples of empirical upper state energies with assignments for Band#4, $\nu_3^1+2\nu_4^2$ ($|l_{eff}|=1$) (full list can be found in Appendix A2).

K′	J′	l_3	l_4	a/s	E′	E′rms	N	Δ*J*=−1				Δ*J*=0				Δ*J*=+1			
								Lower	wn_obs	wn_cal	S_obs	Lower	wn_obs	wn_cal	S_obs	Lower	wn_obs	wn_cal	S_obs
4	6	1	−2	*s*	7034.9848	0.0005	2	PP(7,5)s	6571.9711	6571.9716	1.287E−23	PQ(6,5)s	6710.6133*	6710.6157	1.287E−23	PR(5,5)s	6829.7159	6829.7155	1.287E−23
4	6	−1	2	*s*	7028.7979	0.0003	3	RP(7,3)s	6507.1755	6507.1759	1.287E−23	RQ(6,3)s	6645.4795	6645.4794	1.287E−23	RR(5,3)s	6764.2814	6764.2812	1.287E−23
4	6	−1	2	*a*	7028.4771	0.0003	3	RP(7,3)a	6506.2538	6506.2540	1.287E−23	RQ(6,3)a	6644.4999	6644.4994	1.287E−23	RR(5,3)a	6763.2501	6763.2503	1.287E−23
4	7	1	−2	*s*	7173.7574	0.0007	3	PP(8,5)s	6552.6912	6552.6918	1.287E−23	PQ(7,5)s	6710.7438	6710.7443	1.287E−23	PR(6,5)s	6849.3893	6849.3884	1.287E−23
4	7	−1	2	*a*	7166.3434	0.0013	2	RP(8,3)a	6486.5079	6486.5067	1.287E−23	RQ(7,3)a	6644.1185*	6644.1204	1.287E−23	RR(6,3)a	6782.3645	6782.3658	1.287E−23

Notes:

- Upper state energies (***E***′) and ***E***′rms, and line positions (wn_obs and wn_cal) are in cm^{-1}.
- *N* is the number of transitions used to obtain the empirical upper state energy.
- Line intensities (S_obs) are in $cm^{-1}/(molecule \cdot cm^{-2})$ at 296 K and E−22 means 10^{-22}, etc.
- The upper state quanta are given by K' J' l_3 l_4 *a*/*s*.
- Lower states are the J'', K'' and inversion symmetry (sym).
- For Band#4, proposed to be $\nu_3+2\nu_4^2$, the effective $l_{eff}=l_3+l_4$.
- wn_obs with Flag, "*" are poorly measured positions that are omitted in computing upper state energies.

Most of the good GSCD sets show differences better than ~0.0005 cm^{-1} between the observed line positions and those derived from the newly determined upper state energies. The ground state energies are calculated by Kleiner et al. [21] using Hamiltonian constants reported by Urban et al. [40].

5. Results and discussion

It is emphasized that the GSCD procedure in itself does not provide correct upper state vibrational identities, and sometimes even the upper state *K* and Δ*K*, *l* and inversion symmetry might be different from assumed values. As discussed below, we have used earlier research and recent *ab initio* predictions to infer *tentative band names*; in the future, some of these may be changed once better theoretical calculations are available.

By employing the method of intensity-validated GSCDs described above, we compiled a total of 1096 assignments associated with seven bands; the entire lists are presented by band in Appendix A. Some quantum assignments for four bands ($\nu_1+\nu_3^1$, $2\nu_3^0$, $\nu_1+2\nu_4^2$, and $\nu_3^1+2\nu_4^2$) from the earlier work [31–39] provided a good starting point for our own effort. To confirm assignments and form empirical upper state energies from our line positions, we adopted rather conservative matching criteria (~0.0005 cm^{-1} for unblended and no greater than 0.001 cm^{-1} for blended lines) in order to establish high reliability. In fact, we noticed that some upper state energy levels reported from the earlier work could not be confirmed using these narrow criteria.

An overview of the quantum assignments for seven vibrational bands is presented in Table 8; recalling that the GSCD method alone does not determine the vibrational identity of the upper state, we label the seven bands to be Band no. from #1–#7. The band origins presented with four significant digits below decimal point are those experimentally determined as listed in Table 8. For Band #6, however, our band origin has been crudely derived from the energy levels with low *J* and *K* to be (*s*) 6666.7 and (*a*) 6665.3 cm^{-1} with assumed absolute accuracies that no better than 0.1 cm^{-1}. The proposed band names listed in Table 8 are based on the *ab initio* calculations by HSL-2 [13,14] and TROVE [17]. Following are columns for the number of empirical upper state energy levels and that of assignments in the given frequency ranges with max J values and minimum intensities for the assignments. The last two columns are the band origins predicted by *ab initio* calculations from Huang et al. [13,14] and Yurchenko et al. [17] denoted as HSL-2 and TROVE, respectively, and earlier work [28]. Our experimentally determined Band#3 origins for the symmetric and asymmetric states are (*s*) 6556.4216 and (*a*) 6557.9303 cm^{-1}, respectively; these differ by (*s*) 0.39 and (*a*) 0.38 cm^{-1} from HSL-2 [13,14] and (*s*) 0.20 and (*a*) 0.43 cm^{-1} from TROVE [17], showing somewhat similar degree of discrepancies. However, it is interesting to note that the observed (*a*–*s*) splitting of 1.5087 cm^{-1} shows better agreement with 1.52 cm^{-1} from HSL-2 [13,14] than 1.74 cm^{-1} from TROVE [17], implying the relative precision of line positions calculated by the HSL-2 is quite encouraging.

Table 8
An overview of the quantum assignments from this work.

#	*A/E*	*a/s*	Centers (cm^{-1}) (this work)	Bands	HSL-2	#*E*′	# assign	Freq. range (cm^{-1})	J_{max}	S_{min} (cm $molecule^{-1}$)	HSL-2 [13,14]	TROVE [17]	Expr. [28]
1	*E*	*s*	6608.8220	$\nu_1+\nu_3$ ($\|l\|=1$)	$\nu_3+2\nu_4^0$ ($\|l\|=1$)	137	359	6346.76–6809.39	9	4.15	6610.29	6608.78	6608.83
	E	*a*	6609.7534								6611.22	6609.92	6609.66
2	*A*	*s*		$2\nu_3^0$	$2\nu_3^0$	55	142	6599.33–6973.52	9	6.33	6797.91	6792.83	6795.31
	A	*a*	6795.3384								6796.52	6791.84	6796.73
3	*E*	*s*	6556.4216	$\nu_1+2\nu_4^2$ ($\|l\|=2$)	$\nu_1+2\nu_4^2$ ($\|l\|=2$)	78	180	6377.43–6762.15	7	3.60	6556.80	6556.62	6556.22
	E	*a*	6557.9303								6558.32	6558.36	
4	*E*	*s*	6677.4317	$\nu_3+2\nu_4^2$ ($\|l_{eff}\|=1$)	$\nu_1+\nu_3$ ($\|l\|=1$)	118	293	6401.20–6943.44	9	4.28	6679.36	6677.50	6677.23
	E	*a*	6678.3103								6680.04	6678.12	6677.95
5	*E*	*s*	6850.2449	$2\nu_3^2$ ($\|l\|=2$)	$2\nu_3^2$ ($\|l\|=2$)	34	88	6701.32–6956.51	5	4.60	6850.46	6850.23	6850.20
	E	*a*	6850.6550								6850.86	6850.87	6850.70
6	*E*	*s*	~6666.7	$\nu_3+2\nu_4^0$ ($\|l\|=1$)	$\nu_3+2\nu_4^2$ ($\|l\|=1$)	8	24	6423.61–6772.22	8	5.28	6666.24	6667.66	~ 6666
	E	*a*	~6665.3								6665.77	6668.99	
7	*E*	*s*	6680.9272	$2\nu_2+3\nu_4^1$ ($\|l_{eff}\|=1$)	$5\nu_2+\nu_4$	4	7	6552.62–6770.21	5	47.2	6313.11	6310.83	
	E	*a*	6681.8700		$\nu_1+\nu_3$						6689.33	6679.25	6677.95

Notes:

(1) The 14 columns from left to right are: our band index number (1–7), band type (A=parallel or E=perpendicular for cold bands), symmetry (a or s), band centers in cm^{-1}, ascribed band names, number of empirical upper state energy levels and number of assignments, maximum J values and minimum intensities in 10^{-24} $cm^{-1}/(molecule \cdot cm^{-2})$ at 296 K of the assigned transitions.
(2) The last three columns are the values of predicted band origins from Huang et al. [13,14] and Yurchenko et al. [17] labeled as **HSL-2** and **TROVE**, respectively, and the observations of Coy and Lehmann [28].
(3) The band origins with four significant digits after decimal are derived from an assigned $P(1,K)$, where K=0 or 1.
(4) l_{eff} is defined as l_3+l_4 of the upper state in this work.

As presented in Table 1, there were 381 prior assignments for $\nu_1+\nu_3^1$ and $2\nu_3^0$ by Lundberg-Nielsen et al. [31] and 334 assignments for $\nu_1+2\nu_4^2$, and $\nu_3^1+2\nu_4^2$ by Li et al. [34] and Lees et al. [35], many of which are validated showing a good agreement (ranging from 0.001 cm^{-1} to 0.01 cm^{-1}), and were therefore included among our 1096 assignments, but often with improved precision. At the same time, some earlier assignments did not survive the stringent quality control provided by the empirical lower state energy estimates for individual transitions and the intensity-validated GSCD calculations available to the present study. For instance, of the 47 upper state energies for Band#2 ($2\nu_3^0$) obtained by Xu et al. [33] based on the earlier assignments [31], we saw that of 16 levels differing by more than 0.1 cm^{-1}; three of these were previously flagged as perturbed [33]. For nine other levels (including two given as perturbed), we could not find a consistent set of combination differences to confirm the earlier assignments. In all, we replaced 16 levels, excluded 9, and added 15 new energy assignments, giving a total of 55 assigned levels for the Band#2 ($2\nu_3^0$). For all seven bands, we increased the number of identified upper states by a factor of 1.5.

In Table 9 a list of empirical upper state energies for Band#5 is presented, where the levels for symmetric and asymmetric state are compared with *a–s* splitting in cm^{-1}. As expected with the inversion selection rule for perpendicular bands preventing inversion switching in the transitions, the observed energy level for symmetric states are lower than that of asymmetric states, though their magnitude varies with *J* and *K*. In Table 9, comparison of the (*a–s*) splitting for Band#5 ($2\nu_3^2$) has been added for HSL-2 [13,14] and TROVE [17], where we noticed that the *ab initio* calculations by HSL-2 for the inversion splits agree very well with the empirically determined values in this work, *i.e.* average 0.01 cm^{-1} for most levels. Complete lists of the derived $^{14}NH_3$ empirical upper state energy levels along with (*a–s*) splittings and *l*-doublings (in cm^{-1}) for all seven bands, Bands#1–#7, are presented in Appendix A3.

In Fig. 5, we present a Kitt Peak spectrum (top panel) and seven panels of synthetic spectra computed at the same gas conditions using our observed line parameters of assigned features for six of our seven assigned bands (*in panels* 2–7) and finally for the remaining unassigned line features (*bottom panel*). Only Band#2 is a parallel band, while all others are perpendicular. As seen in Fig. 5, Band#1–#4 are at an acceptable level to reveal broad band features. Integrated line intensities for the assigned transitions for each of the seven bands are computed to be 183, 11.5, 23.1, 68.5, 7.6, 1.7, and 2.60×10^{-21} $cm^{-1}/(molecule\cdot cm^{-2})$ at 296 K, respectively. We note that some of the assignments are blended with stronger features, and some levels are not found so these summations *should not be taken as the true band strengths.* Finally their grand sum of the intensity for the entire assigned transitions over the seven bands is 2.98×10^{-19} $cm^{-1}/(molecule\cdot cm^{-2})$ at 296 K, representing almost two thirds of the total observed intensity (4.68×10^{-19} $cm^{-1}/(molecule\cdot cm^{-2})$ at 296 K in the 6300–7000 cm^{-1} region.

Finally we present a diagram of all the empirical upper state energy levels determined from this work in Fig. 6, where symmetric and asymmetric levels are presented in **red** and **blue** lines, respectively. The star symbols indicate the band origins estimated from our results. The diagram

Table 9
Example of empirical upper state energy levels of $^{14}NH_3$ for Band#5 ($2\nu_3^2$).

K'	J'	l_3	l_4	$E'(s)$ rms (cm^{-1})	$E'(a)$ rms (cm^{-1})	(*a–s*) Obs.	(*a–s*) splitting	
							HSL-2	TROVE
0	1	2	0	6869.4290(05)	6869.8537(02)	0.4246	0.413	0.502
0	2	2	0	6907.7817(02)	6908.2391(01)	0.4574	0.439	0.538
0	4	2	0	7041.7460(04)	7042.3849(01)	0.6389	0.658	0.782
0	5	2	0	7136.8210(03)	7138.1208(01)	1.2997	1.329	1.666
1	2	2	0	6903.3976(02)	6903.8439(01)	0.4463	0.443	0.513
1	4	2	0	7037.3854(04)	7038.0043(05)	0.6189	0.613	0.919
2	2	2	0	6892.3577	6892.7598	0.4021	0.417	0.523
2	3	2	0	6949.8519(00)	6950.2878(01)	0.4358	0.432	0.556
2	4	2	0	7026.4003(06)	7026.9213(03)	0.5210	0.518	0.678
2	5	2	0	7121.8860(07)	7122.5974(05)	0.7114	0.697	0.861
2	2	−2	0	6896.4091(00)	6897.1403(01)	0.7312	0.663	0.478
2	3	−2	0	6953.9195(03)	6954.2291(04)	0.3096	0.286	0.565
2	4	−2	0	7030.4242(01)	7030.9894(06)	0.5652	0.578	0.741
3	5	2	0	7104.3445(03)	7104.8842(03)	0.5397	0.546	0.675
3	3	−2	0	6938.2106(01)	6938.5110(01)	0.3004	0.301	0.498
3	4	−2	0	7014.8624(03)	7015.3421(04)	0.4798	0.490	0.620
4	4	−2	0	6992.4795(00)	6992.8232(10)	0.3437	0.345	0.499
5	5	−2	0	7059.2048(04)	7059.5625(02)	0.3577	0.399	0.487

Notes:

(1) If no rms is listed, then the upper state level is based on only one assignment; if the rms is shown as (00), the level is based on two or more assignments, and the rms is less than 0.00005 cm^{-1}.
(2) The observed values from this work for the Band #5 *a–s* splitting agree very well with those computed by HSL−2 (Huang et al. [13,14] by ~0.01 cm^{-1} for most of the levels measured, while those from TROVE [17] show 0.1–0.3 cm^{-1} offsets.
(3) Full list can be found in Appendix A3.

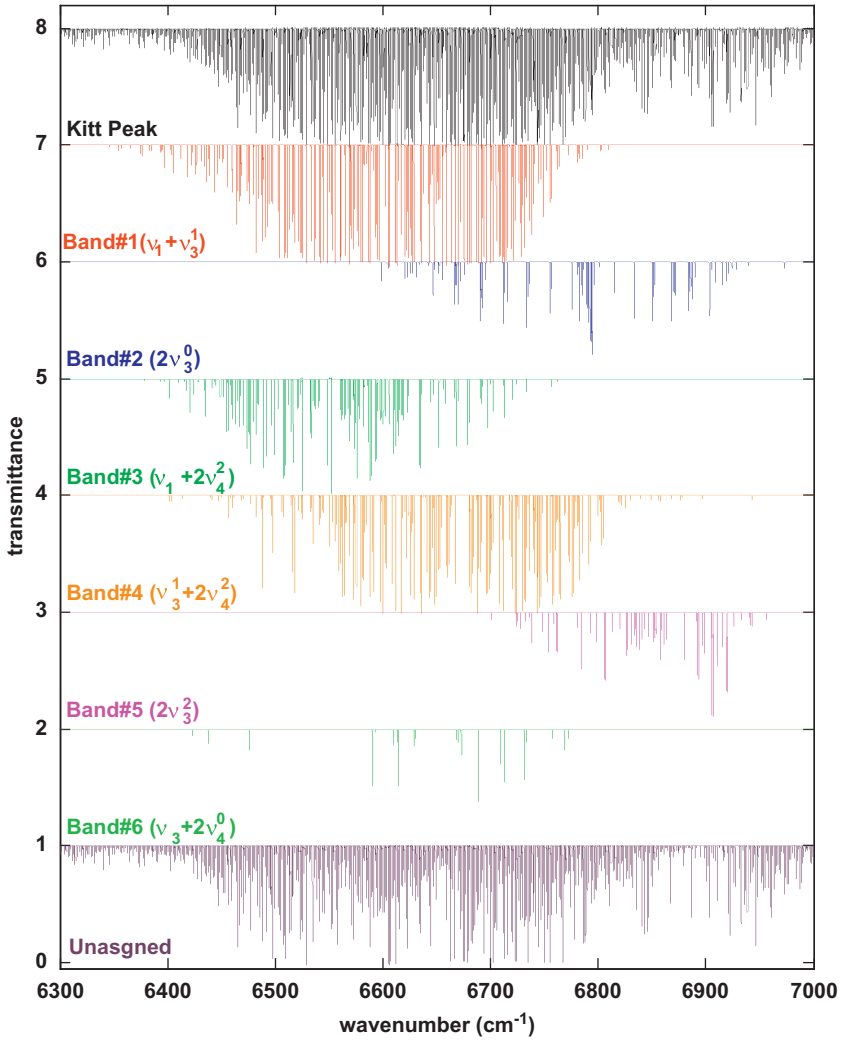

Fig. 5. Observed $^{14}NH_3$ spectrum (top) with several panels of synthetic spectra computed at the same experimental conditions (16.1 m absorption path length, 1.89 Torr, at 296 K). Panels 2–7 show the contributions of six reported bands based on their assignments and measured line parameters; the bottom panel shows the absorption arising from the remaining unassigned features. Note that the few proposed assignments of the 7th band in Table 8 are not presented. The intensity sum of all assigned transitions is ~63% of total measured $^{14}NH_3$ opacity.

can facilitate identifying possible perturbation pairs by noting the neighboring levels of the same *J*.

We have combined and tabulated the measured line positions, line intensities and assignment with tentative band names for ~1000 transitions. A sample of line positions and intensities is presented in Table 10; the entire list for ~4800 lines (excluding known H_2O transitions) is provided as a Supplemental file for the journal. Note that there are only two observed transitions for Band#1 whose intensities are weaker than 5×10^{-24} $cm^{-1}/(molecule\cdot cm^{-2})$, but these are still accepted as valid components of the GSCDs.

6. Caveats

In general, we judge the precision of our individual measurements by the quoted experimental rms of the averages for positions, intensities and empirical lower state energies. However, some computed statistics are too good to be trusted. The very best precisions should be 0.0001 cm^{-1} for positions. These are less reliable if the averaged values are based on retrievals from only one or two spectra listed in Table 3, and also if adjacent features are less than 0.03 cm^{-1} (i.e. blended). In addition, the NH_3 line positions were determined solely from the room temperature spectra, but the effects of self-broadened pressure shifts are not currently characterized at these wavelengths. The apparent shifts can even be both positive and negative for low K transitions [53] retrieved with Voigt line shapes; this can be caused by line mixing between the inversion (*a* and *s*) pairs of perpendicular transitions [53,54]. If the *a* and *s* transitions of parallel bands are well separated, the pressure shifting tends to be more 'ordinary', with shifts becoming increasingly more negative with increasing *J* [55]. The effect on our line centers is crudely estimated by assuming that shifts are

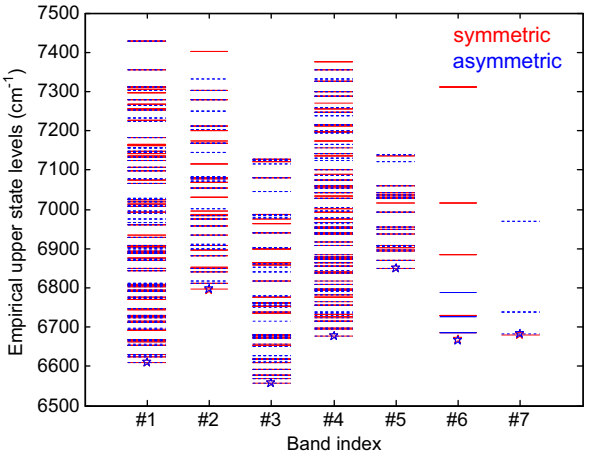

Fig. 6. A diagram of all empirical upper state energy levels determined in this work (with symmetric and asymmetric levels in a **red** and a **blue** line, respectively). The star symbols represent the band origins estimated from current assignments. (For interpretation of the references to color in this figure legend, the reader is referred to the web version of this article.)

approximately one-tenth of the self-broadened widths; for a large width of $\sim$0.6 cm^{-1} atm^{-1} [53,56], the self-shift would be 0.06 cm^{-1} atm^{-1} (similar large shifts are seen in H_2O [57]). Thus, a line center might be pressure-shifted by -0.0008 cm^{-1} if only the two high pressure scans (10 and 8.5 Torr) were used to obtain the averaged line centers, while the self-shift would be 10 times smaller with the 0.8 Torr scan.

For line intensities, there are more opportunities for major systematic errors (as discussed by Birk et al. [58]). The %rms given in the linelist can indicate the *experimental precision* of the measured line intensity if the average is based on four or more spectra. Any computed %rms less than 3% should be viewed with suspicion, however. A successful theoretical modeling of intensities is needed to know if the quoted precisions are generally reliable. With ammonia, there are additional problems with the behavior of the gas inside the sample chamber that can degrade the *absolute accuracy*. A reasonable expectation is that the overall absolute accuracy is better than 10%, but this can be confirmed only by comparison with other independent measurements. We do note that many of the same scans were used to obtain values at 2 μm [43] and so the intensities of the two regions are likely to be consistent.

The empirical lower state energies E'' obtained using the cold data do provide helpful clues for assigning transitions. Their experimental precisions often range from 5% to 20% for *unblended* features (as confirmed by the assignments). For *blends*, the uncertainties of intensities at room and cold temperatures (see Table 3) tend to degrade the resulting E''. While the rms of the averaged E'' values from individual measurements for each feature is computed, but this value is not always reliable (especially for very weak features in the linelist). A value greater than 1000 cm^{-1} is particularly suspect because a weak feature may be a blend of multiple transitions. In the Supplemental file, the lower state energies of assigned lines are replaced with theoretically calculated values based on the quantum numbers. For others, the experimental lower states are inserted in order to enable further assignments.

To validate the linelist, direct comparisons of observed and synthetic spectra were done to check positions and intensities at room temperature. Some poorly characterized blended features were then remeasured using knowledge of the quantum assignments. For example, some blends were assigned as the two asymmetry components of transitions and so the new retrieval was initialized using two lines of equal intensity with equal self-broadened widths for the quantum assignment. In other cases, the blend contained one component of an asymmetric pair, and the measured intensity of the unblended partner was used to initiate a new retrieval. This permitted a number of faults to be corrected, but not always. For example, the PQ(J,1) branch near 6612 cm^{-1} proved intractable for retrieving reliable positions and intensities, even when starting with *ab initio* calculated intensities. In the end, we remeasured this Q branch in one low optical density spectrum by holding fixed the positions based on the available empirical upper levels and adjusted only the individual line intensities. However, this special treatment did not produce a reliable retrieval.

Finally, the present laboratory spectra contained unwanted features arising from water vapor at low pressure inside the FTS chamber. The retrievals were initiated using linelists generated by peak-finding and thus some H_2O lines were measured using the molecular weight of ammonia. The identified H_2O lines are intentionally removed in our database, but it is possible that some ammonia transitions are hidden by the water.

7. Conclusion

We measured line positions and line intensities of $^{14}NH_3$ for $\sim$4800 features in the 6300–7000 cm^{-1} from multiple sets of Kitt Peak spectra recorded at various low temperatures. We found that sum of the line intensities in the region is 4.68×10^{-19} cm^{-1}/(molecule$\cdot$cm^{-2}) at 296 K, representing 99.7% of the total opacity in this spectral interval. We estimated lower state energies of 3567 observed lines by measuring their line intensities at different temperatures; these values and an *ab initio* prediction permitted us to select new quantum assignments and confirm existing ones in the literature using the GSCD method. We report a total of 1096 allowed transitions in a composite database, along with empirical upper state energies for 434 levels associated with seven different vibrational states, inferred from *ab initio* calculations [13,14,17]. The new assigned positions will provide good experimental constraints to improve $^{14}NH_3$ *ab initio* calculations (by the Ames group). For example, a preliminary refinement of the Potential Energy Surface (PES) using $\sim$20 selected energy levels has already produced very promising agreement between new predictions and observed values. As presented in Fig. 7, these 0.02–0.03 cm^{-1} rms errors suggest that at least 80% of assignments reported in this work are reliable. More

Table 10
Example of measured $^{14}NH_3$ line parameters with quantum assignments (full list can be found in Appendix A4).

MMi	wn	Strength	A	b_air b_slf	Edn	nT	delta	Vup	(J K l_3 l_4)′ –(J K l_3 l_4)″	E''(est.)	%E''	N1	N2	unc(pos)	%S	wn(o-c)	Flag
111	6711.5623	3.200e−23	0.0	0.0650.4500		0.75	0.000000						2	0.00131	11.0		
111	6711.6430	1.666E−23	0.0	0.0650.4500	413.2378	0.75	0.000000	1002a	7 0 0 2 − 6 1 0 0 PR(6,1)a	320.0	9.4	2	2	0.00004	3.5	0.0004	A
111	6711.6856	1.766E−23	0.0	0.0650.4500	588.0	0.75	0.000000			588.0	1.0	2	2	0.00011	2.6		
111	6711.7705	3.722E−22	0.0	0.0650.4500	194.9063	0.75	0.000000	1010s	5 0 −1 0 − 4 1 0 0 PR(4,1)s	210.0	7.7	8	6	0.00022	4.9	0.0017	C
111	6711.7705	0.000E+00	0.0	0.0650.4500	195.6113	0.75	0.000000	1010a	5 0 −1 0 − 4 1 0 0 PR(4,1)a	210.0	7.7	8	6	0.00022	4.9	−0.0016	C
111	6711.8451	1.524E−23	0.0	0.0650.4500	225.0	0.75	0.000000			225.0	2.1	2	2	0.00029	7.0		
111	6711.9310	2.045E−22	0.0	0.0650.4500	199.2939	0.75	0.000000	0020s	3 0 0 0 − 4 0 0 0 QP(4,0)a	214.0	5.3	6	5	0.00015	3.0	0.0000	A
111	6711.9839	8.792E−22	0.0	0.0650.4500	44.7960	0.75	0.000000	0012s	3 3 −1 2 − 2 2 0 0 RR(2,2)s	63.0	5.5	4	6	0.00009	3.7	−0.0004	A
111	6712.2947	6.860E−23	0.0	0.0650.4500	195.6113	0.75	0.000000	0020s	3 1 0 0 − 4 1 0 0 QP(4,1)a	557.0	9.2	6	2	0.00084	5.7	−0.0014	*
118	6712.3077	3.660e−22	0.0	0.0650.4500	251.0	0.75	0.000000			251.0	7.3	6	2	0.00011	1.8		
111	6712.3664	1.049E−22	0.0	0.0650.4500	194.9063	0.75	0.000000	0020a	3 1 0 0 − 4 1 0 0 QP(4,1)s	208.0	8.4	6	4	0.00028	3.1	−0.0001	A
111	6712.4970	1.319E−23	0.0	0.0650.4500	490.0	0.75	0.000000			490.0	4.9	2	2	0.00063	13.5		
111	6712.6354	1.682E−22	0.0	0.0650.4500	16.1730	0.75	0.000000	0012s	2 0 −1 0 − 1 1 0 0 PR(1,1)s	39.0	3.9	3	6	0.00031	3.2	−0.0000	A
111	6712.6993	1.835E−23	0.0	0.0650.4500	453.0	0.75	0.000000			453.0	3.9	2	2	0.00055	3.4		
111	6712.7645	5.162E−22	0.0	0.0650.4500	294.6300	0.75	0.000000	1010a	6 2 1 0 − 5 1 0 0 RR(5,1)a	312.0	8.7	10	6	0.00025	3.8	0.0002	A
111	6712.7972	2.859E−23	0.0	0.0650.4500	1167.0	0.75	0.000000			1167.0	0.0	1	2	0.00002	15.2		
111	6712.9498	1.097E−21	0.0	0.0650.4500	293.9683	0.75	0.000000	1010s	6 2 1 0 − 5 1 0 0 RR(5,1)s	390.0	9.0	7	5	0.00086	4.3	0.0000	E
111	6712.9965	7.582E−22	0.0	0.0650.4500	489.0	0.75	0.000000			489.0	8.5	8	5	0.00102	4.7		
111	6713.1457	4.517E−24	0.0	0.0650.4500		0.75	0.000000						1	0.00000	0.0		
118	6713.3102	3.150e−23	0.0	0.0650.4500	566.0	0.75	0.000000			566.0	1.4	2	3	0.00048	2.3		
111	6713.3750	8.040E−23	0.0	0.0650.4500	412.6243	0.75	0.000000	1002s	7 0 0 2 − 6 1 0 0 PR(6,1)s	252.0	1.6	2	4	0.00043	3.7	0.0006	B
111	6713.3883	6.380E−23	0.0	0.0650.4500	183.8291	0.75	0.000000	0020a	3 2 0 0 − 4 2 0 0 QP(4,2)s	252.0	1.6	2	4	0.00043	3.7	0.0056	*
111	6713.3883	0.000E+00	0.0	0.0650.4500	265.2267	0.75	0.000000	1002a	6 2 0 2 − 5 3 0 0 PR(5,3)a	252.0	1.6	2	4	0.00043	3.7	−0.0050	*
111	6713.4209	8.120E−23	0.0	0.0650.4500	184.5531	0.75	0.000000	0020s	3 2 0 0 − 4 2 0 0 QP(4,2)a	148.0	6.4	5	4	0.00049	3.1	−0.0001	A
111	6713.4782	1.754E−23	0.0	0.0650.4500	353.0	0.75	0.000000			353.0	5.3	2	2	0.00050	4.1		
111	6713.5059	9.518E−24	0.0	0.0650.4500		0.75	0.000000						2	0.00012	6.3		

Notes: The parameters are listed in a pseudo-HITRAN format:

MM=molecular code, 11 for NH_3.
i=all lines are for $^{14}NH_3$. Values other than $i=1$ are codes indicating that we remeasured lines.
wn=observed or calculated position in cm^{-1} depending on their quality code (See below).
S=strength in $cm^{-1}/(molecule \cdot cm^{-2})$ at 296 K.
b_air, b_slf, nT=assumed air- and self-broadened widths, the temperature dependence parameter for b_air.
delta=assumed air-pressure-induced frequency shift.
Vup=upper state vibrational band notation by ($v1$,$v2$,$v3$,$v4$). '1002' should read as v_1+2v_4.
Edn=lower state energies:
Those having four significant digits below decimal point are the lower state energies adopted from Urban et al. [40], based on the quantum assignment made in this work.
Those having one significant digits below decimal point are copy of E''(est.).

E''(est.)=empirical lower state energy estimates derived from cold data (See text for details).
%E''=percentage uncertainties associated with the E''(est.).
N1=# of spectra averaged to get the mean E''(est.).
N2=# of spectra averaged to get the mean position.
unc.(pos)=uncertainty in the position in cm^{-1} for the given transition.
wn(o-c)=wn_obs-wn_cal, where wn_cal=$\boldsymbol{E}'-E''$.
%S=percentage uncertainty of the line intensities. '0.0' means 'not available'.
Flag=Quality code (see below).
A for $|wn(obs\text{-}cal)| \le 0.0005\ cm^{-1}$; B for $|wn(obs\text{-}cal)| \le 0.001\ cm^{-1}$; C for $|wn(obs\text{-}cal)| \le 0.005\ cm^{-1}$;
D for $|wn(obs\text{-}cal)| > 0.005\ cm^{-1}$; E for $|wn(obs\text{-}cal)|$, not available.
for transitions omitted in the calculation of the upper state energy, for which wn_cal is listed.

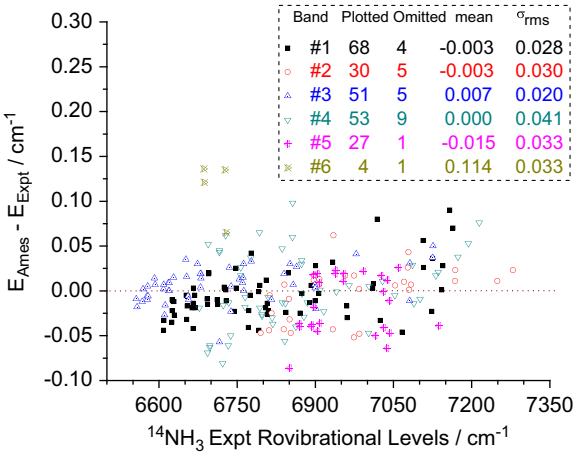

Fig. 7. Agreement between selected observed energy levels and those predicted with a refined *ab initio* calculation (by the HSL group) for six bands. The inset panel gives the number of levels plotted and outliers omitted, along with the mean and σ_{rms} values in cm^{-1} for the plotted values. It is noted that a few larger outliers are omitted because large deviations (e.g. the largest being 1.12, 2.48, 0.81, −2.67, −0.10, −5.43 cm^{-1} for Band #1–#6, respectively) may indicate an incorrect vibrational identity. Note that only 23 of all 32 blocks of $J=0$–7 levels are included in this comparison.

importantly, a unique part of this work is the close collaboration between the high resolution experimental analysis and the full-dimensional quantum computations.

In summary, the intensity arising from just these assigned lines represents two-thirds of the total observed opacity for the region. These data can guide further improvements to the theoretical models. In addition, like N_2, NH_3 is a major carrier of nitrogen in various atmospheres of extrasolar planets [10] and ultra-cool ($T<\sim$600 K) brown dwarfs [9,59], whose atmospheric properties can be better studied through infrared photospectrometric observations using ground-, aircraft- and space-based observatories (IRTF, NSPIRES (Keck II telescope), SOFIA, HST, and later JWST [60], etc.) with a view to supporting remote sensing of (exo)planets, and brown dwarfs, and other astrophysical environments as well as the atmosphere of the Earth. The entire list of the spectroscopic line parameters and quantum assignments are provided to the journal as electronic supplements.

8. Future work

As seen in Table 11, there are several strong bands (e.g., $2\nu_1$, $4\nu_4^2$, $\nu_1+2\nu_2+\nu_4$, $\nu_1+2\nu_4^0$, etc.) still to be located. Experimental work on this region is also in progress by other researchers [61–63], who are also applying the GSCD procedure to their own cold spectra, guided by available theoretical (*ab initio*) predictions [eg., 13,14,17]. It is hoped that through these collective efforts, this region of ammonia will finally be fully characterized.

There is a logical sequence for new studies. The forbidden transitions for known vibrational states must be cataloged, and the intensity prediction for such lines validated and improved. Then weaker transitions of additional vibrational states (e.g., $\nu_1+2\nu_4$, $2\nu_1$, $\nu_1+2\nu_2+\nu_4$, $4\nu_4$, etc.) can be identified with trustworthy predictions of line positions based on new successfully refined PES (by the Ames group) with valid constraints obtained in this work. Transitions of the very weakest bands will more likely be found by searching simultaneously for the corresponding hot bands vibrations at longer wavelength. Locating all 43 vibrational states may be very difficult, however. In the interim, the empirical NH_3 database from the present study will be continually updated to provide detailed knowledge for high resolution applications. Later this year an updated composite linelist with estimated broadening parameters will be submitted for inclusion in the public (HITRAN [22] and GEISA [23]) databases. A discussion of intensities will be the subject of a future paper, along with new quantum assignments afforded by improved theoretical models.

Table 11
Sum of predicted *ab initio* intensities from Yurchenko et al. [16,17].

Band	l_3	l_4	$\sum$ ints (s−state)	$\sum$ ints (a−state)	$\sum$ all ($a+s$)	Number of lines		
						(s)	(a)	($a+s$)
Identified								
1010	1	0	7.728	8.543	16.27	634	645	1279
1002	0	2	6.068	3.120	9.19	1553	1564	3117
0020	2	0	0.791	0.770	1.56	1465	464	929
0020	0	0	0.659	0.638	1.298	297	281	578
0012	1	2	0.233	0.267	0.500	355	345	700
0012	1	0	n/a[&]					
0203	0	1	0.173	2.780	2.952	515	525	1040
Unidentified								
1002	0	0	0.612	0.577	1.189	657	650	1307
1201	0	1	1.043	0.485	1.528	998	955	1953
2000	0	0	0.167	0.146	0.313	325	315	640
0004	0	2	0.290	0.282	0.572	1009	1007	2016
0402	0	0	0.060	0.020	0.081	205	211	416
0211	1	1	0.074	0.053	0.071	420	459	879
0310	1	0	0.0005	0.094	0.094	105	136	241

Notes:

(1) Intensity sums are in units of 10^{-20} $cm^{-1}/(molecule\cdot cm^{-2})$ at 296 K using transitions stronger than 5×10^{-22} $cm^{-1}/(molecule\cdot cm^{-2})$.
(2) The line intensities are adopted from TROVE database [16,17] (http://www.tampa.phys.ucl.ac.uk/ftp/astrodata/NH3).
(3) The columns are vibrational upper state, l_3 and l_4 (assumed by us), integrated line intensities for s, a, $a+s$ combined, respectively, in $cm^{-1}/(molecule\cdot cm^{-2})$ at 296 K, number of lines included for s and a states and total number, respectively, for the given band.
(4) Band notation 1010 should be read as $\nu_1+\nu_3$.
(5) Considered to be part of $\nu_3+2\nu_4$ in the summation of line strengths.

Acknowledgments

This paper is dedicated to our friends and colleagues Drs. Jean-Marie Flaud, Claude Camy-Peyret and Alain Barbed for their invaluable guidance and prolific research in theoretical and experimental molecular spectroscopy and also atmospheric remote sensing. They long ago joined the ranks of spectroscopists who work simply for the fun of understanding complex spectra. The research at the Jet Propulsion Laboratory (JPL) is performed under

contract with National Aeronautics and Space Administration. The first author (K. Sung) thanks Drs. Li-Hong Xu and Ronald M. Lees at University of New Brunswick for providing the electronic files of their NH_3 energy levels. The AMES group also thanks Drs. Li-Hong Xu and Ronald M. Lees for helpful discussions. The Ames group gratefully acknowledges support from the NASA Grants 08-APRA08-0050 and 10-APRA10-0096. X. Huang acknowledges the support by NASA/SETI Institute Co-operative Agreement, NNX09AI49A. K. Lehmann acknowledges the support from the National Science Foundation and from NASA.

Appendix A. Supporting information

Supplementary data associated with this article can be found in the online version at doi:10.1016/j.jqsrt.2012.02.037.

References

[1] Wildt R. Ultrarote Absorption band en in den Spektra der grossen Planeten. Naturwissenschaften 1931;19:109.
[2] Gillett FC, Low FJ, Stein WA. 2.8–14 μm spectrum of Jupiter. Astrophys J 1969;157:925–34.
[3] Hanel RA, Conrath BJ, Flasar FM, Herath LW, Kunde VG, Lowman P, et al. Infrared observations of the Jovian system from Voyager 2. Science 1979;206:952–6.
[4] Carlson R, Weissman P, Smythe WD, Mahoney JC, the NIMS Science and Engineering Team. Near-infrared mapping spectrometer experiment on Galileo. Space Sci Rev 1992;60:457–502.
[5] Carlson R, Smythe W, Baines K, Barninis E, Becker K, Burns R, et al. Near-infrared spectroscopy and spectral mapping of Jupiter and the Galilean satellites: results from Galileo's initial orbit. Science 1996;274:385–8.
[6] Flasar FM, Kunde VG, Abbas MM, Ade P, Barucci A, Bézard B, et al. Exploring the Saturn system in the thermal infrared: the composite infrared spectrometer. Space Sci Rev 2004;115:169–297.
[7] Saumon D, Marley MS, Leggett SK, Golimowski DA, Cushing MC, Fan X, et al. Physical parameters of two very cool T dwarfs. Astrophys J 2007;656:1136–49.
[8] Leggett SK, Cushing C, Saumon D, Marley MS, Froellig TL, Warren SJ, et al. The physical properties of four similar to 600 K T dwarfs. Astrophys J 2009;695:1517–26.
[9] Leggett SK, Marley MS, Freedman R, Saumon D, Liu MC, Geballe TR, et al. Physical and spectral characteristics of the T8 and later type dwarfs. The physical properties of four similar to 600 K T dwarfs. Astrophys J 2007;667:537–48.
[10] Sudarsky D, Burrows A, Hubeny I. Theoretical spectra and atmospheres of extrasolar giant planets. Astrophys J 2003;588:1121–48.
[11] Line MR, Vasisht G, Chen P, Angerhausen D, Yung YL. Thermochemical and photochemical kinetics in cooler hydrogen-dominated extrasolar planets: a methane-poor GJ436b. Astrophys J 2011;738:32–46.
[12] Huang X, Schwenke DW, Lee TJ. An accurate global potential energy surface, dipole moment surface, and rovibrational frequencies for NH_3. J Chem Phys 2008;129:214304.
[13] Huang X, Schwenke DW, Lee TJ. Rovibrational spectra of ammonia. I. Unprecedented accuracy of a potential energy surface used with nonadiabatic corrections. J Chem Phys 2011;134:044320, doi:10.1063/1.3541351.
[14] Huang X, Schwenke DW, Lee TJ. Rovibrational spectra of ammonia. II. Detailed analysis, comparison, and prediction of spectroscopic assignments for $^{14}NH_3$, $^{15}NH_3$, and $^{14}ND_3$. J Chem Phys 2011;134:044321.
[15] Yurchenko SN, Zheng J, Lin H, Jensen P, Thiel W. Potensital-energy surface for the electronic ground state of NH_3 up to 20,000 cm^{-1} above equilibrium. J Chem Phys 2005;123:134308, doi:10.1063/1.2047572.
[16] Yurchenko SN, Barber RJ, Yachmenev A, Thiel W, Jensen P, Tennyson J. A variationally computed $T=300$ K line list for NH_3. J Phys Chem A 2009;113:11845–55.
[17] Yurchenko SN, Barber RJ, Tennyson J, Thiel W, Jensen P. Towards efficient refinement of molecular potential energy surfaces: ammonia as a case study. J Mol Spectrosc 2011;268:123–9.
[18] Pickett HM. The fitting and prediction of vibration–rotation spectra with spin interactions. J Mol Spectrosc 1991;148:371–7.
[19] Chen P, Pearson JC, Pickett HM, Matsuura S, Blake GA. Measurements of $^{14}NH_3$ in the $v_2=1$ state by a solid-state, photomixing, THz spectrometer, and a simultaneous analysis of the microwave, terahertz, and infrared transitions between the ground and v_2 inversion—rotation levels. J Mol Spectrosc 2006;236:116–26.
[20] Yu S, Pearson JC, Drouin BJ, Sung K, Pirali O, Vervloet M, et al. Submillimeter-wave and far-infrared spectroscopy of high-J transitions of the ground and $v_2=1$ states of ammonia. J Chem Phys 2010;133:174317.
[21] Kleiner I, Tarrago G, Cottaz C, Sagui L, Brown LR, et al. NH_3 and PH_3 line parameters: the 2000 HITRAN update and new results. J Quant Spectrosc Radiat Transfer 2003;82:293–312.
[22] Rothman LS, Gordon IE, Barbe A, Benner DC, Bernath PF, Birk M, et al. The HITRAN 2008 molecular spectroscopic database. J Quant Spectrosc Radiat Transfer 2009;110:533–72.
[23] Jacquinet-Husson N, Crepeau L, Armante R, Boutammine C, Chédin A, Scott NA, et al. The 2009 edition of the GEISA spectroscopic database. J Quant Spectrosc Radiat Transfer 2011;112:2395–445.
[24] Irwin PGJ, Calcutt SB, Sihra K, Taylor FW, Weir AL, Ballad J, et al. Band parameters and k coefficients for self-broadened ammonia in the range 4000–11,000 cm^{-1}. J Quant Spectrosc Radiat Transfer 1999;62:193–204.
[25] Strong K, Taylor FW, Calcutt SB, Remedios JJ, Ballard J. Spectral parameters of self- and hydrogen-broadened methane from 2000 to 9500 cm^{-1} for remote sounding of the atmospheric Jupiter. J Quant Spectrosc Radiat Transfer 1993;50:363–429.
[26] Goody R, West R, Chen L, Crisp D. The correlated-k method for radiation calculations in nonhomogenous atmospheres. J Quant Spectrosc Radiat Transfer 1989;42:539–50.
[27] Benedict WS, Plyler EK. Vibration–rotation bands of ammonia 2. The molecular dimensions and harmonic frequencies of ammonia and deuterated ammonia. Can J Phys 1957;35:1235–41.
[28] Coy SL, Lehmann KK. Rotational structure of ammonia N–H stretch overtones—5 and 6 quanta bands. J Chem Phys 1986;84:5239–49.
[29] Coy SL, Lehmann KK. Modeling the rotational and vibrational structure of the IR and optical-spectrum of NH_3. Spectrochim Acta A—Mol Biomol 1989;45:47–56.
[30] Lehmann KK, Coy SL. Spectroscopy and intramolecular dynamics of high excited vibrational states of NH_3. J Chem Soc Faraday Trans 1988;84:1389–406.
[31] Lundsberg-Nielsen L, Hegelund F, Nicolaisen FM. Analysis of the high-resolution spectrum of ammonia ($^{14}NH_3$) in the near-infrared regions, 6400–6900 cm^{-1}. J Mol Spectrosc 1993;162:230–45.
[32] Berden G, Peeters R, Meijer G. Cavity-enhanced absorption spectroscopy of the 1.5 μm band system of jet-cooled ammonia. Chem Phys Lett 1999;307:131–8.
[33] Xu L-H, Liu Z, Yakovlev I, Tretyakov MY, Lees RM. External cavity tunable diode laser NH_3 spectra in the 1.5 μm region. Infra Phys Technol 2004;45:3–45.
[34] Li L, Lees RM, Xu L-H. External cavity tunable diode laser spectra of the $\nu_1+2\nu_4$ stretch-bend combination bands of $^{14}NH_3$ and $^{15}NH_3$. J Mol Spectrosc 2007;243:219–26.
[35] Lees RM, Li L, Xu L-H. New VISTA on ammonia in the 1.5 μm region: assignments for the $\nu_3+2\nu_4$ of $^{14}NH_3$ and $^{15}NH_3$ by isotopic shift labeling. J Mol Spectrosc 2008;251:241–51.
[36] O'Leary DM, Orphal J, Ruth AA, Heitmann U, Chelin P, Fellows CE. The cavity-enhanced absorption spectrum of NH_3 in the near-infrared region between 6856 and 7000 cm^{-1}. J Quant Spectrosc Radiat Transfer 2008;109:1004–15.
[37] Jia H, Zhao W, Cai T, Chen W, Zhang W, Gao X. Absorption spectroscopy of ammonia between 6526–6538 cm^{-1}. J Quant Spectrosc Radiat Transfer 2009;110:347–56.
[38] Webber ME, Baer DS, Hanson RK. Ammonia monitoring near 1.5 μm with diode-laser absorption sensors. Appl Opt 2001;40:2031–42.
[39] Czajkowski A, Alcock AJ, Bernard JE, Madej AA, Corrigan M, Chepurov S. Studies of saturated absorption and measurements of optical frequency for lines in the $\nu_1+\nu_3$ and $\nu_1+2\nu_4$ bands of ammonia at 1.5 μm. Opt Exp 2009;17:9258–69.
[40] Urban Š, D'Cunha R, Rao NK, Papousek D. The $\Delta K=\pm 2$ forbidden band and inversion rotation energy-levels of ammonia. Can J Phys 1984;62:1775–91.

[41] Urban Š. Effective rotational Hamiltonians of pyramidal XY_3 molecules with the inversion splitting of energy levels. J Mol Spectrosc 1988;131:133–53.
[42] Pracna P, Špriko V. Electric dipole moment function of ammonia. J Mol Spectrosc 1989;136:317–32.
[43] Brown LR, Margolis JS. Empirical line parameters of NH_3 from 4791 to 5294 cm^{-1}. J Quant Spectrosc Radiat Transfer 1996;56:283–94.
[44] Kleiner I, Brown LR, Tarrago G, Kou Q-L, Picque N, Guelachvili G, et al. Positions and intensities in the $2\nu_4$, ν_1 and ν_3 vibrational system of NH_3 near 3 μm. J Mol Spectrosc 1999;193:46–71.
[45] Pollock CR, Petersen FR, Jennings DA, Wells JS, Maki AG. Absolute frequency measurements of the 2–0 band of CO at 2.3 μm; calibration standard frequencies from high resolution color center laser spectroscopy. J Mol Spectrosc 1983;99:357–68.
[46] Picque N, Guelachvili G. Absolute wavenumbers and self-induced pressure lineshift coefficients for the 3–0 vibration–rotation band of $^{12}C^{16}O$. J Mol Spectrosc 1997;185:244–8.
[47] Brown LR, Margolis JS, Norton RH, Stedry B. Computer measurements of line strengths with application to the methane spectrum. Appl Spectrosc 1983;37:287–92.
[48] Humlicek J. Optimized computation of the Voigt and complex probability functions. J Quant Spectrosc Radiat Transfer 1982;27: 437–44.
[49] Lees RM, Li L, Liu Z, Xu L-H. External cavity tunable diode laser spectrum of the $\nu_1+\nu_3$ N–H stretching combination band of $^{15}NH_3$. J Mol Struct 2006;795:134–42.
[50] Lins B, Pflaum F, Engelbrecht R, Schmauss B. Absorption line strengths of $^{15}NH_3$ in the near infrared spectral region. Appl Phys B 2011;102:293–301.
[51] Gamache RR, Kennedy S, Hawkins R, Rothman LS. Total internal partition sums for molecules in the terrestrial atmosphere. J Mol Struct 2000;517/518:407–25.
[52] Fabian M, Yamada KMT. Absolute intensity of the NH_3 ν_2 band. J Mol Spectrosc 1999;198:102–9.
[53] Markov VN, Pine AS, Buffa G, Tarrini O. Self broadening in the ν_1 band of NH_3. J Quant Spectrosc Radiat Transfer 1993;50:167–78.
[54] Henck SA, Lehmann K. Coherence transfer between rotation inversion transitions in the ν_3 fundamental of NH_3. Chem Phys Lett 1988;144:281–5.
[55] Guinet M, Jeseck P, Mondelain D, Pepin I, Janssen C, Camy-Peyret C, et al. Absolute measurements of intensities, positions and self-broadening coefficients of R branch transitions in the ν_2 band of ammonia. J Quant Spectrosc Radiat Transfer 2011;112:1950–60.
[56] Gibb JS, Hancock G, Peverall R, Ritchie GAD, Russell LJ. Diode laser based detection and determination of pressure-induced broadening coefficients in the $\nu_1+\nu_3$ combination band of ammonia. Eur Phys J D 2004;28:59–66.
[57] Toth RA, Brown LR, Plymate C. Self-broadened widths and frequency shifts of water vapor from 590 to 2400 cm^{-1}. J Quant Spectrsoc Radiat Transfer 1998;59:529–62.
[58] Birk M, Hausamann D, Wagner G, Johns JWC. Determination of line strengths by Fourier-transform spectroscopy. Appl Opt 1996;35: 2971–85.
[59] Burrows A, Marley M, Hubbard WB, Lunine JI, Guillot T, Saumon D, et al. A nongray theory of extrasolar giant planets and brown dwarfs. Astrophys J 1997;491:856–75.
[60] Posselt W, Holota W, Kulinvak E, Kling G, Kutscheid T, Le Fevre O, et al. NIRSpec: near-infrared spectrograph for the JWST. In: Mather JC, editor. Optical, infrared, and millimeter space telescopes, Orlando, vol. 5487. SPIE; 2004. p. 688–97.
[61] Cacciani P, Cermak P, Cosléu J, Jeseck P, Michaut X. New progress in spectroscopy of ammonia in the infrared 1.5 μm range using evolution of spectra from 300 K down to 122 K. J Quant Spectrosc Radiat Transfer, doi:10.1016/j.jqsrt.2012.02.026, in press.
[62] Down MJ, Hill C, Barber RJ, Yurchenko SN, Tennyson J. Assignment of infrared ammonia spectra. Poster O3, HRMS, Dijon Fr.; 2011.
[63] Berg DJ, Degman DA, Davidson KL, Dyer SW, Fristoe CR, Griswold G, et al. Diode laser absorption spectrum of cold bands of NH_3 at 6500 cm^{-1}. Poster N8, HRMS, Dijon Fr.; 2011.